JOURNAL OF PROPULSION AND POWER
Vol. 27, No. 1, January–February 2011

Thermochemical Erosion Analysis for Graphite/Carbon–Carbon Rocket Nozzles

Daniele Bianchi,* Francesco Nasuti,† and Marcello Onofri‡
University of Rome "La Sapienza," 00184 Rome, Italy
and
Emanuele Martelli§
Second University of Naples, 81131 Caserta, Italy

DOI: 10.2514/1.47754

A study is conducted to predict graphite/carbon–carbon nozzle erosion behavior in solid rocket motors for wide variations of propellant formulations. The numerical model considers the solution of Reynolds-averaged Navier–Stokes equations in the nozzle, heterogeneous chemical reactions at the nozzle surface, variable transport and thermodynamic properties, and heat conduction in the nozzle material. Two different ablation models are considered and compared: a surface equilibrium approach and a finite-rate model. Results show that the erosion rate is diffusion limited for metallized propellants, ensuring sufficiently high wall temperatures, and it is kinetic limited for nonmetallized propellants. For low surface temperatures, the two models are consistent with each other and predict the same erosion rate, while the surface equilibrium model overpredicts the recession at low surface temperatures. The calculated results show an excellent agreement with the experimental data from the ballistic test and evaluation system motor firings, and the finite-rate model actually improves the predictions when the kinetic-limited regime is approached.

Nomenclature

A	=	cross-section area, m^2
D_{im}	=	effective diffusion coefficient, m^2/s
e_0	=	total energy per unit mass, J/kg
h	=	enthalpy, J/kg
k	=	thermal conductivity, $W/m \cdot K$
$\dot{m}$	=	mass blowing rate per unit area, $kg/m^2 \cdot s$
N_c	=	number of species
p	=	pressure, N/m^2
r	=	distance from surface, m
$\dot{s}$	=	erosion rate, m/s
T	=	temperature, K
t	=	time, s
u	=	streamwise velocity, m/s
$\mathbf{u_i}$	=	diffusion velocity of species i, m/s
v	=	velocity component normal to surface, m/s
$\mathbf{v}$	=	mass motion of the mixture, m/s
$\mathbf{v_i}$	=	mass motion of species i, m/s
W	=	molecular weight, kg/kmol
y	=	mass fraction
y^+	=	dimensionless wall distance
ΔH_{abl}	=	heat of ablation, J/kg
η	=	outward coordinate normal to surface
μ	=	viscosity, $kg/m \cdot s$
μ_t	=	turbulent viscosity, $kg/m \cdot s$
ρ	=	density, kg/m^3
$\dot{\omega}_i$	=	species source term in control surface, $kg/m^2 \cdot s$

Subscripts

c	=	combustion chamber
eq	=	surface equilibrium model
f-r	=	finite-rate model
i	=	species
s	=	solid (carbon) properties at gas/solid interface
w	=	gas properties at gas/solid interface

Presented as Paper 2009-4977 at the 45th AIAA/ASME/SAE/ASEE Joint Propulsion Conference and Exhibit, Denver, CO, 2–5 August 2009; received 22 October 2009; revision received 30 June 2010; accepted for publication 29 August 2010.

*Research Fellow, Department of Mechanics and Aeronautics, via Eudossiana 18. Student Member AIAA.
†Associate Professor, Department of Mechanics and Aeronautics, via Eudossiana 18. Senior Member AIAA.
‡Full Professor, Department of Mechanics and Aeronautics, via Eudossiana 18. Senior Member AIAA.
§Assistant Professor, Department of Aerospace and Mechanical Engineering, via Roma 29. Student Member AIAA.

I. Introduction

WITH the development of high-energy solid propellants and harder firing conditions in advanced solid rocket motors (SRMs), graphite and carbon–carbon composites have found increasing application in SRM nozzles because of their excellent thermal and physical properties and low densities. However, the hostile thermochemical environment resulting from the high-performance solid propellants creates many problems to such materials. One of the serious problems is the erosion/recession of the rocket nozzle material. As the propellant of the rocket-motor burns, the nozzle is exposed to the hot propellant combustion products that form a turbulent boundary layer over the nozzle surface. The hot products transfer energy to the nozzle wall, causing the surface temperature to rise, and hence increasing the reactivity of the nozzle material. At high surface temperatures, heterogeneous chemical reactions occur between the nozzle material and oxidizing species such as H_2O and CO_2, normally found in a significant amount in the combustion stream. Heterogeneous reactions consume the oxidizing species at the nozzle surface and produce carbon monoxide CO: the result is the thermochemical erosion of the nozzle. Such erosion is most severe at the throat due to the maximum heat-transfer rate in that region. As the nozzle throat area increases, thrust decreases, and thus the motor performance reduces, especially in long-duration firings. The classic way to measure performance reduction is to test full-scale motors, but this takes a long time and is very expensive, because tests must be repeated for every new motor. A complementary method is to establish regression models that can accurately predict the regression rate of the nozzle throat, but these models

require a fundamental knowledge of the major mechanisms that drive the regression rate.

The identification and description of the major mechanisms governing nozzle erosion has been the subject of many investigations [1–8] in solid rocket technology. As mentioned previously, the most reactive gases are H_2O and CO_2, which react with carbon to form carbon monoxide. The overall rate of these reactions depends on their kinetics as well as on the rate at which the oxidizing species can diffuse across the boundary layer to the nozzle surface. If the kinetic rates are much higher than the diffusion rates, the recession rate is determined primarily by the diffusion mechanism of oxidizing species (diffusion limited). The other extreme situation is that of high diffusion rates and low kinetic rates, in which case the recession is predominantly determined by the chemical kinetics (kinetic limited). It has been found [3,6,7] that the erosion is kinetic controlled when the surface temperature is below a transition temperature. Above this value, which is highly dependent on the chemical kinetics and can sometimes be as high as 2800 K [7], the chemical reactions become sufficiently fast to consume all the oxidizing species diffusing to the surface; thus, the local chemical equilibrium is established at the solid–gas interface. When such a condition is reached, the erosion process is considered diffusion limited, and the solution is no longer dependent on the kinetic rates of the heterogeneous surface reactions. The diffusion-limited condition is usually reached for metallized propellants while, for a nonmetallized propellant that has lower flame temperatures and higher concentrations of oxidizing species, the surface temperature can fall below the transition temperature, and chemical kinetic rates may control the recession process [6,7]. In such a case, the diffusion-limited calculations would overestimate the erosion rate. Therefore, a full nonequilibrium model is required for the most general case, which needs the knowledge of the controlling reactions as well as their rate constants. The diffusion-limited erosion depends on such parameters as flow properties in the nozzle, the chamber pressure, and the concentrations of the reactants. The kinetic-limited erosion depends on the constants of the heterogeneous reactions, the concentrations of the various reactants, and especially the surface temperature of the nozzle. The surface temperature is determined by the surface energy balance (SEB), which involves the heat transfer from the hot gases to the nozzle, the heat conduction response of the nozzle material, and the heat flux absorbed by the ablation mechanism. The overall nozzle erosion process is extremely complex with the interplay of numerous factors, including the solid-propellant composition, motor operating conditions, duration of firing, nozzle geometry and material properties, rates of diffusion of the species toward the surface through the boundary layer, and chemical reactions at the surface and in the gas phase. Finally, some material may be lost by sublimation of the carbon itself, as pointed out by Klager [1], even if sublimation can be considered of minor importance as an ablation mechanism, because SRM nozzles typically operate at temperatures too low to activate oxidation/sublimation transition [8]. In addition to the aerothermochemical processes, the erosion may have contributions from the mechanical processes caused by the impact of condensed metal-oxide particles (e.g., Al_2O_3) on the nozzle surface or by the structural failure because of high thermal stresses. However, it has been shown that the chemical erosion is the primary reason for the nozzle recession [1,9].

The objective of this study is to formulate and validate a comprehensive model based on a full Navier–Stokes approach coupled with a surface thermochemical ablation model for predicting the thermochemical erosion rate of a graphite/carbon–carbon nozzle and to study the effect of propellant composition on the erosion process. In particular, in the present paper, a finite-rate ablation model is implemented on a verified Reynolds-averaged Navier–Stokes equations solver [10,11]. This solver has been recently validated with a surface equilibrium ablation model for diffusion-limited ablation test cases [8]. In this study, two baseline propellants for studying the nozzle erosion process have been selected. One propellant is a nonmetallized propellant, and the other is a metallized propellant. Both are ammonium perchlorate/hydroxyl-terminated polybutadiene (AP/HTPB) composite propellants.

II. Theoretical Modeling

The theoretical formulation for nozzle recession rate predictions has been developed and validated in [8]. The earlier version of this model was validated by using experimental data obtained by Geisler [2] from the ballistic test and evaluation system (BATES) rocket-motor firings. The gas-phase dynamics are based on the full Navier–Stokes equations for single-phase multicomponent reacting systems, where variable thermodynamic and transport properties are accounted for. The heat conduction process in the nozzle is treated as being one dimensional and steady state. The surface chemical erosion model has been updated from a chemical equilibrium approach to a finite-rate chemistry approach.

A. Governing Equations for Gas Phase

The governing equations for the gas phase are the reacting turbulent Reynolds-averaged Navier–Stokes equations [12]:

$$\begin{cases} \frac{\partial \rho y_i}{\partial t} + \nabla \cdot (\rho y_i \mathbf{v_i}) = \dot{w}_i & i = 1, \ldots, N \\ \frac{\partial \rho}{\partial t} + \nabla \cdot (\rho \mathbf{v}) = 0 \\ \frac{\partial (\rho \mathbf{v})}{\partial t} + \nabla \cdot (\rho \mathbf{v}\mathbf{v}) - \nabla \cdot \mathbf{S} = 0 \\ \frac{\partial (\rho e_0)}{\partial t} + \nabla \cdot (\rho e_0 \mathbf{v}) = \nabla \cdot (\mathbf{v} \cdot \mathbf{S}) - \nabla \cdot \mathbf{q} \end{cases} \tag{1}$$

where $\mathbf{v_i}$ is the mass motion of species i, which can be expressed as

$$\mathbf{v_i} = \mathbf{v} + \mathbf{u_i} \tag{2}$$

where $\mathbf{v}$ is the mass motion of the mixture, and $\mathbf{u_i}$ is the diffusion velocity of species i.

The term $\mathbf{S}$ is the stress tensor, split into the contribution of pressure forces and viscous stresses, the term $\mathbf{q}$ is the heat flux vector, and the term $\dot{w}_i$ is the source term due to chemical reaction:

$$\mathbf{S} = -p\mathbf{I} + \mathbf{T} \qquad \mathbf{T} = -\tfrac{2}{3}\mu(\nabla \cdot \mathbf{v})\mathbf{I} + \mu[\nabla \mathbf{v} + (\nabla \mathbf{v})^T] \tag{3}$$

$$\mathbf{q} = -k\nabla T + \sum_{i=1}^{N} h_i \rho y_i \mathbf{u_i}$$

where $\mathbf{I}$ is the unit tensor. The diffusional mass flux of the ith species $\mathbf{j}_i$ can be expressed using the approximation of Fick's law:

$$\mathbf{j}_i = \rho y_i \mathbf{u_i} = -\rho D_{\text{im}} \nabla y_i \tag{4}$$

Variable transport and thermodynamic properties are taken into account. The thermodynamic properties of individual species are approximated by seventh-order polynomials of temperature while the transport properties are approximated by fourth-order polynomials [13]. Mixture properties for conductivity and viscosity are derived from the Wilke's rule. The diffusion model is based on a single global diffusion coefficient obtained assuming a constant Lewis number. For the present study, it is important to stress that the two following major assumptions are made:

1) Radiation heat transfer is negligible.

2) Gas-phase reactions have a negligible effect on the recession process (frozen flow in the gas phase).

The first assumption is made because radiation is usually one order of magnitude less than convection in rocket nozzle applications [3,5]. The second assumption is justified by literature studies [4,7] showing that the nozzle recession process is rather independent of gas-phase reactions.

B. Governing Equations for Solid Phase

It is assumed that heat conduction into the nozzle material is dominant in the radial direction. Although temperature gradients exist along the nozzle wall, these are generally small if compared with the radial heat conduction and represent a second-order effect, which has not been accounted for in the present analysis. In a moving local coordinate system tied to the receding surface, the temperature

distribution at a given distance r from the surface is governed by the following equation [6,14]:

$$\rho_s \frac{\partial h_s}{\partial t} = \frac{1}{A}\frac{\partial}{\partial r}\left(k_s A \frac{\partial T_s}{\partial r}\right) + \rho_s \dot{s}\frac{\partial h_s}{\partial r} \tag{5}$$

The terms in Eq. (5) represent, from left to right, the sensible energy accumulation, the net conduction, and the net energy convected as a consequence of coordinate motion. A closed-form solution of the heat conduction equation at steady state [15,16] is available, integrating Eq. (5) between the nozzle–gas interface and the nozzle outer wall, assuming an adiabatic condition for the latter and steady-state condition ($\partial \cdot / \partial t = 0$). This approximation is made in the present study, because the heating of the nozzle material in the SRM environment is very quick [3,17]: the surface temperature rises rapidly in less than 1 s of exposure and then increases very slowly with time, denoting an almost steady-state condition.

C. Gas/Surface Boundary Conditions

Because of the chemically active surface, further physical modeling is necessary for the gas/surface interaction. To complete the formulation of the theoretical model, boundary conditions must be specified at the gas/solid interface that describe the physics of the surface phenomena.

1. *Mass and Energy Balances*

Consider the fluxes of mass/energy entering and leaving a control surface fixed to the ablating surface. The solid material may be visualized as moving into the surface at a rate $\dot{s} = \dot{m}/\rho_s$. If it is assumed that no material is being removed in a condensed phase (solid or liquid), then the general surface mass/energy balances for a chemically reacting, graphitic ablating surface can be written as [16]

$$\rho D_{\text{im}} \frac{\partial y_i}{\partial \eta}\bigg|_w + \dot{\omega}_i = (\rho v)_w y_{i_w}, \qquad i = 1, N_c \tag{6}$$

which is the surface mass balance (SMB) for the ith species, and

$$k\frac{\partial T}{\partial \eta}\bigg|_w + \sum_i^{N_c} h_{i_w} \rho D_{\text{im}} \frac{\partial y_i}{\partial \eta}\bigg|_w + \dot{m} h_s = (\rho v)_w h_w - k_s \frac{\partial T_s}{\partial r}\bigg|_s \tag{7}$$

which is the SEB.

The terms on the left-hand side of Eq. (6) are the mass fluxes of species i entering the surface due to diffusion and heterogeneous surface reactions, respectively, while the term on the right-hand side is the mass flux of species i leaving the surface due to surface ablation. The source term $\dot{\omega}_i$ is positive for the ablation products and negative for the oxidizing species, which are consumed in the ablation process.

The terms on the left-hand side of Eq. (7) are the heat fluxes entering the surface due to conduction from gas, diffusion, and surface motion, respectively, while the terms of the right-hand side are the heat fluxes leaving the surface due to surface ablation and conduction in the material. The conduction term $-k_s \partial T_s/\partial r$ is represented by a closed expression available at steady state from Eq. (5). Thus, the solid- and gas-phase boundaries are coupled at the interface.

A summation of Eq. (6) over all the species yields the total mass rate:

$$\sum_i \dot{\omega}_i = (\rho v)_w = \dot{m} = \rho_s \dot{s} \tag{8}$$

Now, introducing in Eq. (6) the variable $y_{i_s} = \dot{\omega}_i/\dot{m}$, which is the mass of species i produced or consumed in the ablation process per unit mass of the material ablated, and substituting Eq. (6) into Eq. (7) yields a compact form of the SEB:

$$k\frac{\partial T}{\partial \eta}\bigg|_w - \dot{m}\Delta H_{\text{abl}} = -k_s \frac{\partial T_s}{\partial r}\bigg|_s \tag{9}$$

The term

$$\Delta H_{\text{abl}} = \left(\sum_i h_{i_w} y_{i_s} - h_s\right)$$

is the so-called heat of ablation, which is the difference between the enthalpies of the species created or consumed by the ablation process and the enthalpy of the solid material at the surface temperature per mass of material removed.

The other boundary conditions at the solid–gas interface are

$$u = 0, \qquad v = \dot{m}/\rho, \qquad \partial p/\partial \eta|_w = 0 \tag{10}$$

The surface energy and mass balances, Eqs. (6) and (9), permit us to evaluate the ablation mass rate and the surface temperature, once they are coupled with a proper chemical model to describe the surface reactions.

2. *Heterogeneous Reaction Kinetics*

In this work, the results of two approaches are analyzed: a chemical equilibrium model and a finite-rate erosion formulation. The first approach has been extensively described in [8,18] and is based on the hypothesis that local chemical equilibrium is established at the solid–gas interface; hence, the erosion process is assumed diffusion limited. The finite-rate model described herein is more general and includes the diffusion-limited condition.

At high temperatures, the carbon surface is prone to chemical attack by the oxidizing species present in the combustion gases. The most reactive gases are those that react with carbon to form carbon monoxide. Gases such as H_2O, CO_2, OH, NO, O, and O_2 react with carbon to form CO. However, NO, O, and O_2 are present in very low concentrations in typical propellant combustion products, so their erosion contribution can be neglected. Concerning the alumina particles, even though the reaction of carbon with Al_2O_3 is thermodynamically slightly favored in the temperature range of interest, the overall contribution to nozzle erosion of the alumina–carbon reaction appears to be small due to its slow kinetics involving condensed-phase reactants. For such a reason, from a chemical standpoint, alumina has been treated as an inert species. In addition to chemical erosion, there could be contributions from mechanical processes associated with impingement of alumina particles on the nozzle surface. The mechanical erosion caused by the impingement of Al_2O_3 particles is negligible in the throat region and downstream, as the particles travel almost parallel to the surface. The effect may be of interest in the converging part of the nozzle, but the erosion of this region is not as crucial as the throat erosion and, hence, has been neglected. The most important oxidizing species for graphite/carbon–carbon is water vapor, due to its considerable amount in the exhaust gases, ranging from 10% (metallized propellant) up to 30% (nonmetallized propellant). Thus, H_2O, CO_2, and OH are considered to be the only major reactive species [3,7], and they are assumed to react with carbon, as shown by the following reactions:

$$\text{C}_s + \text{H}_2\text{O} \rightarrow \text{CO} + \text{H}_2 \tag{11}$$

$$\text{C}_s + \text{CO}_2 \rightarrow 2\text{CO} \tag{12}$$

$$\text{C}_s + \text{OH} \rightarrow \text{CO} + \text{H} \tag{13}$$

The rate of erosion of carbon by an oxidizing species i can be expressed as

$$\dot{m}_i = p_i^n \cdot A_i T_w^b \exp(-E_i/RT_w) \tag{14}$$

where p_i is the partial pressure of the oxidizing species i, T_w is the surface temperature, and n is the overall order of the heterogeneous reaction. A_i and E_i are the pre-exponential factor and the activation energy of the heterogeneous reaction, respectively. In the present study, the kinetic parameters of Eq. (14) are taken from [7] and listed in Table 1.

Table 1 Kinetic data for heterogeneous surface reactions

Surface reaction	A_i	E_i, kcal/mol	b	n
$C_s + H_2O \rightarrow CO + H_2$	4.8×10^5	68.8	0.0	0.5
$C_s + CO_2 \rightarrow 2CO$	9.0×10^3	68.1	0.0	0.5
$C_s + OH \rightarrow CO + H$	3.61×10^2	0.0	−0.5	1.0

In practice, the reaction rates should also depend on the specific type of graphite/carbon–carbon and the associated manufacturing processes, but the chemical kinetics for carbon–carbon and graphite are assumed to be the same in the present work. However, differences in densities and enthalpies are retained in the formulation. The sublimation of carbon is not considered in the kinetic approach, since it has been shown that such a phenomena is not activated in practical rocket-motor environment [8]. The total erosion rate of carbon due to the surface heterogeneous reactions is

$$\dot{m} = \dot{m}_{H_2O} + \dot{m}_{CO_2} + \dot{m}_{OH} = \rho_s \dot{s} \tag{15}$$

where ρ_s is the density of the solid carbon, and $\dot{s}$ is the erosion velocity. The chemical source terms in Eq. (6), $\dot{\omega}_i$, are defined as

$$\dot{\omega}_{CO} = \dot{m}_{H_2O}(W_{CO}/W_C) + \dot{m}_{CO_2}(2W_{CO}/W_C) + \dot{m}_{OH}(W_{CO}/W_C)$$
$$\dot{\omega}_{CO_2} = -\dot{m}_{CO_2}(W_{CO_2}/W_C), \qquad \dot{\omega}_{H_2O} = -\dot{m}_{H_2O}(W_{H_2O}/W_C)$$
$$\dot{\omega}_{OH} = -\dot{m}_{OH}(W_{OH}/W_C), \qquad \dot{\omega}_{H_2} = \dot{m}_{H_2O}(W_{H_2}/W_C)$$
$$\dot{\omega}_H = \dot{m}_{OH}(W_H/W_C)$$
$$\dot{\omega}_i = 0 \quad \text{for } i = HCl, N_2, \quad \text{and} \quad Al_2O_3 \tag{16}$$

With the wall pressure coming from the flowfield (assuming zero-pressure gradient at wall) and with the wall temperature computed from the SEB in Eq. (9), the chemical composition at the nozzle wall and the net erosion rate can be obtained from Eqs. (6) and (14–16).

For the diffusion-controlled recession process, the concentration of oxidizing species at the gas/solid interface is very small (i.e., $y_{i_w} \approx 0$). For such a case, Eq. (6) dictates that the chemical source term equals the diffusive mass flux. On the contrary, when the recession is kinetically controlled, the oxidizing species concentration at wall is nonzero so that a part of the incoming diffusive mass flux reacts with the solid carbon, and a part is convected away from the wall due to blowing. The species equations (6) are solved for the mass fractions of all the species at wall without the need of any control procedure to switch from diffusion-limited to kinetic-limited erosion. Such a procedure, in fact, is not needed if the SMB is correctly integrated with the flow solver: the mass flux of oxidizing species consumed by surface reactions can never exceed the diffusive mass flux, because their sum is always positive according to Eq. (6). Since the surface mass and energy balances are intimately coupled, they must be solved jointly.

III. Numerical Procedure

The analysis of the SRM nozzle flowfield is performed by a two-dimensional axisymmetric time-accurate multispecies Reynolds-averaged Navier–Stokes solver [11,19,20]. The solver is based on a second-order finite difference approach validated and verified in the past [10,11,21]. The Spalart–Allmaras one-equation model [22] is used to compute the turbulent viscosity μ_t. Turbulent conductivity and turbulent mass diffusivity are computed from μ_t, specific heat at constant pressure, turbulent Prandtl number (a standard value of 0.9 is assumed), and turbulent Schmidt number (a standard value of 0.9 is assumed). All computations are made considering bulk graphite ($\rho_s = 1.83$ g/cm^3) as the nozzle material, for which the thermodynamic properties as a function of temperature are taken from literature data [13]. The ablation mass rate is computed from the SMB in Eq. (6) and the finite-rate ablation model in Eqs. (14–16). Once the ablation mass rate has been computed, the erosion rate can be easily derived from Eq. (8), obtaining $\dot{s} = \dot{m}/\rho_s$. The surface temperature is computed from the SEB in Eq. (9) using Newton's iterative procedure. At each computational fluid dynamics (CFD) iteration, the surface temperature, the erosion rate, and the wall chemical composition are continuously updated until a steady-state condition is reached. This procedure has permitted us to carry out all the computations presented in the following without introducing any further numerical treatment to increase code robustness. All computations have been carried out with a suitable choice of y^+ and verified by a grid convergence analysis.

The computational domain is defined by the nozzle geometry. The nozzle is characterized by subsonic inflow boundary conditions describing the combustion chamber (total temperature and total pressure are enforced together with the flow direction and chemical composition), supersonic outflow, symmetry axis, and solid wall. The inlet flow is a mixture of gases derived from chemical equilibrium calculations.

IV. Results and Discussion

The model described in the preceding sections is implemented to simulate the nozzle erosion in practical SRM environments. The nozzle geometry employed is the one used in the BATES rocket motor, and it has been rebuilt on the basis of the main geometric parameters (throat radius, overall dimensions, and divergence angle) reported in [9]. The 70 lb BATES motor is shown in Fig. 1. As shown in Fig. 2a, the adopted grid geometry has been modified with respect to the real nozzle geometry. The BATES nozzle, in fact, is made of a conical convergent section with an angle of 45°, which would have caused a certain ambiguity in imposing the inflow boundary condition due to the unknown velocity direction at the inlet. For that reason, the convergent section has been reproduced using a parabolic curve, which becomes parallel to the nozzle axis at the inlet section so that an axial inlet velocity profile can be assigned. Since the length of the wall is important, because it affects the boundary-layer thickness and hence the heat and mass transfer rate, the total wall length of the parabolic curve is equal to that of the 45° cone. Nozzle material is described according to the BATES nozzle erosion test (bulk graphite). The outside nozzle wall temperature is 300 K for all computations. The hot exhaust gas flowing in the nozzle consists of the combustion products of typical AP/HTPB composite propellants. For metallized propellants, a single-phase treatment is used in the model, so all the Al_2O_3 present in the exhaust gas is assumed to be in the gas phase. The computational domain is subdivided into 60×70 grid points in the axial and radial directions, respectively (Fig. 2a). In the radial direction, meshes are clustered near the nozzle surface to ensure a value of y^+ less than 1.0 all along the nozzle length to accurately capture the near-wall phenomena. All the computations presented are at the steady-state condition obtained by iterating in time until residuals drop by five orders of magnitude. To ensure that the presented results are grid independent, the CFD solution has been verified by a grid convergence analysis on three grid levels for one of the validation test cases, which is discussed in the following. The finest mesh has 120×140 cells in the axial and radial directions, respectively. Each mesh coarsening is made by removing one node out of two in each coordinate direction. Table 2 shows a comparison between the erosion rate evaluated with the three grid levels at three different locations: $x = 7.35$ cm (peak erosion rate), $x = 8.21$ cm (throat section), and $x = 9.58$ cm (beginning of

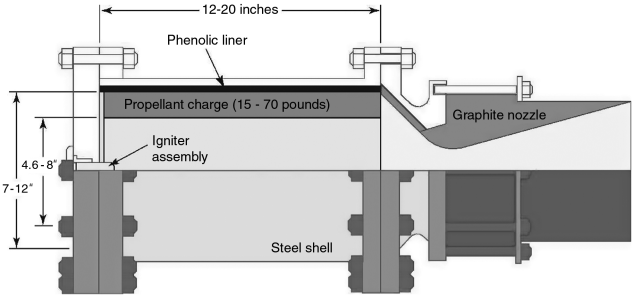

Fig. 1 70 lb BATES motor [9].

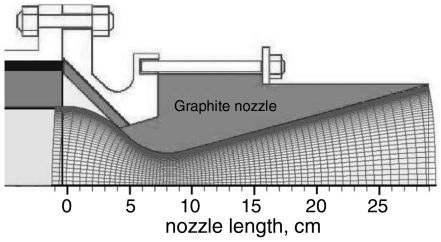

a) Nozzle grid

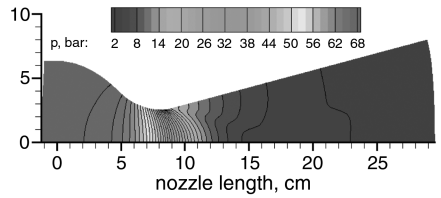

b) Pressure field

Fig. 2 Numerical simulation of BATES motor nozzle flow.

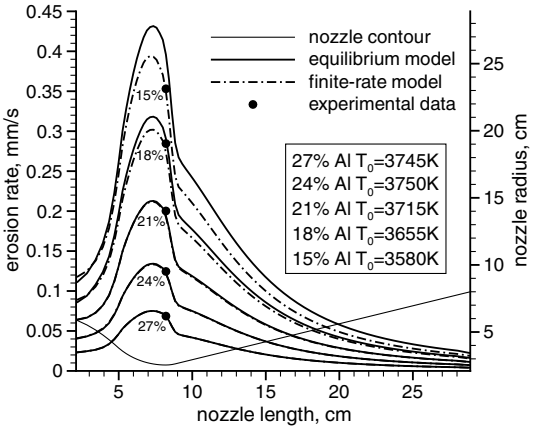

Fig. 3 Erosion rate distribution for propellants with different aluminum contents.

the conical divergent section). The quantitative analysis of solutions obtained on three grid levels confirms that the spatial order of accuracy is close to the formal value. This confirms the asymptotic behavior of the numerical error and thus gives a good confidence on the error estimate. The discrepancy between the erosion rate evaluated with the medium and fine grids is less than 1.5% at the throat location; therefore, the medium grid has been selected for the validation and analysis test cases.

A. Validation by Bates Motor Experimental Data

To validate the current model, calculated recession rates have been compared with the BATES motor experimental data from Geisler [2] and Geisler and Beckman [9] for five different propellant compositions with wide variations of aluminum content and flame temperature (Table 3, [23]).

The computed erosion rate distributions along the nozzle length as a function of the aluminum content of the propellant are plotted in Fig. 3 together with the experimental data measured at the throat. The results obtained with the surface equilibrium model have been extensively discussed in [8]. In the present work, the same calculations have been performed with the finite-rate ablation model. The calculated surface temperature profiles for the five aluminized propellants are plotted in Fig. 4. The surface temperatures are higher for propellants with higher aluminum content due to the combined effect of higher flame temperature and lower erosion rate due to the lower amount of oxidizing species available. The kink visible in the wall temperature distribution is due to the change of curvature between the throat and the conical divergent section of the nozzle, and it is driven by the wall pressure, which also shows a sharp discontinuity in the same position. The high thermal conductivity of graphite would smooth such a sharp discontinuity, but in the present approach, the solid thermal model has been simplified assuming one-dimensional conduction in the radial direction. The erosion rates at the throat computed with the surface equilibrium assumption show an excellent agreement with the experimental data, except for the propellant with the minimum aluminum content. This trend has been explained in [8], noting that the 15% aluminum propellant exhibits a rather low wall temperature (below 2800 K), where the influence of chemical kinetics can be important, which would explain the overestimate of the erosion rate computed with the surface equilibrium. This explanation is now further confirmed with the results obtained using the finite-rate model. Figure 3 clearly shows that the erosion predictions with the finite-rate model are exactly like their surface equilibrium counterparts for the higher aluminum content propellants. The finite-rate erosion in the case of 15 and 18% aluminum propellants is lower than the corresponding surface equilibrium erosion, resulting in a better agreement with the experimental data. In particular, for the 15% aluminum propellant, the equilibrium model provides a 12% overestimation compared to the 1% underestimation provided by the finite-rate model. The comparison between the experimental and the computed erosion rates at the throat is also reported in Table 4 for both the surface equilibrium and the finite-rate model.

These results show that, for metallized propellants ensuring sufficiently high wall temperatures, a surface equilibrium assumption is a valid approximation, and the finite-rate model predicts a diffusion-limited erosion regime. For lower surface temperatures, however, the chemical kinetics become important and control the overall erosion process. When the process is kinetic limited, the erosion rate is reduced, and the surface temperature is consequently increased if compared with the corresponding surface equilibrium computations, as Fig. 4 clearly shows. The lower the surface temperature, the more the surface equilibrium predictions overestimate the actual erosion rates.

It is also important to stress that, in the diffusion-limited regime, the wall temperature has a minor influence on the erosion rate, whereas the opposite is true in the kinetic-limited regime. This is because wall temperature, which is controlled by the flame

Table 2 Grid convergence analysis

Grid	$\dot{s}$, mm/s ($x = 7.35$ cm)	$\dot{s}$, mm/s ($x = 8.21$ cm)	$\dot{s}$, mm/s ($x = 9.58$ cm)
30×35	0.294022	0.261987	0.167377
60×70	0.301885	0.273677	0.173536
120×140	0.304005	0.277737	0.174986

Table 3 Mass fractions, pressure, temperature, and aluminum content for validation of experiments by Geisler [23]

y_{CO}	y_{CO_2}	y_{HCl}	y_{H_2}	y_{H_2O}	y_{N_2}	$y_{Al_2O_3}$	p_c, bar	T_c, K	Al, %
0.175	0.04	0.24	0.02	0.145	0.10	0.28	69	3580	15
0.18	0.025	0.23	0.02	0.105	0.10	0.34	69	3655	18
0.20	0.015	0.195	0.02	0.07	0.10	0.40	69	3715	21
0.20	0.005	0.190	0.02	0.045	0.10	0.44	69	3750	24
0.20	0.005	0.190	0.02	0.025	0.10	0.46	69	3745	27

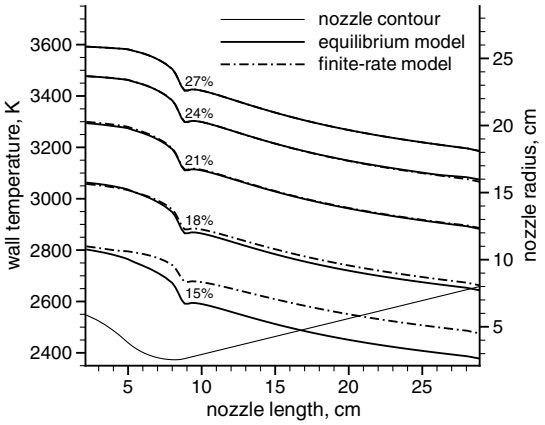

Fig. 4 Wall temperature distribution for propellants with different aluminum contents.

temperature, does not affect the species diffusion in the boundary layer, while it can strongly influence the rate of erosion [see Eq. (14)]. To confirm this, the flame temperature of the 15 and 27% Al propellants has been artificially lowered from its original value (3580 and 3745 K, respectively) to a much lower value of 3000 K. The 15 and 27% Al propellants have been selected because the erosion rate is kinetic limited for the first and diffusion limited for the latter. The effect of the flame temperature reduction is shown in Fig. 5: the lower flame temperature has a direct effect on the surface temperature, but it only affects the erosion rate in the kinetic-limited regime (15% Al propellant). The good agreement of the predictions with the BATES experimental data using the finite-rate model, which is strongly influenced by surface temperature, also confirms that the surface temperature (and hence the SEB) is realistically reproduced.

B. Analysis of Results

In this analysis, two baseline propellants from the experiments reported in [24] have been selected to study the nozzle erosion process. One propellant is a metallized propellant, and the other is a nonmetallized propellant for which the mass fractions are shown in Table 5. These mass fractions have been determined by chemical equilibrium calculations at a chamber pressure of 69 bar in [7]. It can be noted that the exhaust gas equilibrium composition changes noticeably when aluminum is added to the propellant: this is because aluminum consumes most of the oxygen in the propellant to form Al_2O_3 and other aluminum oxides. Thus, a lower amount of oxidizing species is available in the exhaust gas. The numerical computations performed with the two erosion models (equilibrium vs finite rate) for the two propellant formulations show almost no differences in the core-flow region (Fig. 2b). The main differences are experienced in the boundary layer and at the nozzle surface; therefore, the attention will be directed toward the boundary-layer structure in the presence of ablation.

Table 4 Comparison between calculated and experimental data for throat recession

Al, %	$\dot{s}_{\text{expt}}$, mm/s	$\dot{s}_{\text{eq}}$, mm/s (error%)	$\dot{s}_{\text{f-r}}$, mm/s (error%)
15	0.3531	0.3958 (+12%)	0.3497 (−1)
18	0.2845	0.2907 (+2.2%)	0.2737 (−3.8)
21	0.2000	0.1943 (−2.9%)	0.1926 (−3.7)
24	0.1245	0.1226 (−1.5%)	0.1218 (−2)
27	0.0686	0.0684 (<1%)	0.0684 (<1)

Table 5 Nozzle inlet flow conditions

Species	Mass fractions (metallized AP/HTPB)	Mass fractions (nonmetallized AP/HTPB)
CO	0.23	0.11
CO_2	0.02	0.22
HCl	0.20	0.267
H_2	0.01	0.003
H_2O	0.09	0.29
N_2	0.10	0.10
OH	0.01	0.01
Al_2O_3	0.34	——
	Motor conditions	
$T_c(K)$	3500	3000
p_c, bar	69	69

The effect of the two different ablation models is first analyzed, comparing the results for the two selected propellants. Figure 6a shows the total erosion rate for the metallized propellant and the contribution to the net erosion rate due to the three main oxidizing species according, to Eq. (15), which can be divided for the material density ρ_s, leading to

$$\dot{s} = \dot{s}_{H_2O} + \dot{s}_{CO_2} + \dot{s}_{OH} \tag{17}$$

The total erosion rate can therefore be expressed as the sum of the contribution of each oxidizing species. The maximum erosion rate, experienced a bit ahead of the throat, is slightly reduced (3.5%) when using the finite-rate ablation model instead of the surface equilibrium ablation. Looking at the erosion contribution of the three oxidizing species, it can be noted that this reduction is mainly due to carbon dioxide, for which the erosion contribution is reduced in the finite-rate approach. This is due to the relatively slow kinetic of the CO_2 reaction in Eq. (12), if compared with the other surface reactions. This result is further stressed by Fig. 6b, which shows the oxidizing species mass fractions at the surface. A clear indicator of whether or not the erosion is in the diffusion-limited regime is the mass fraction of the oxidizing species at the surface. The more it is close to zero, the more the diffusion-limited regime is attained. The finite-rate model yields nearly zero H_2O and OH wall mass fractions; on the contrary, the CO_2 wall mass fraction is nonzero, denoting that the erosion contribution from this oxidizing species is kinetic limited (Fig. 6b). The wall mass fraction of the oxidizing species is zero for the surface equilibrium model, because the chemical equilibrium assumption forces all the available oxidizing species at the surface to be entirely consumed.

Figures 6c and 6d show the wall temperature and pressure distributions with the finite rate and equilibrium models for the metallized propellant. The knee visible in the wall temperature distribution is due to the change of curvature between the throat and the conical divergent section of the nozzle. Clearly, the pressure profile is unaffected by the surface ablation model. The wall temperature instead shows an increase when using the finite-rate model. This can be explained, considering that the surface reactions are endothermic; hence, the more the surface erodes, the more heat is absorbed by the ablation process. Since the finite-rate model predicts a slightly lower erosion rate, the surface temperature is, consequently, slightly increased. It is also interesting to note that the temperature increase is more pronounced downstream of the throat section, where the difference between the two models is more evident, due to the lower surface temperature. Looking at Fig. 6a, in fact, the erosion rate predicted by the two models is nearly the same in the convergent section, where the surface temperature is rather high, while it is different in the throat and divergent sections, where the surface temperature diminishes. Looking at Figs. 6a and 6c, the results show that the transition temperature between diffusion-limited and kinetic-limited erosions is approximately 2800 K.

Figure 7 shows the same results as Fig. 6, but for the nonmetallized propellant case. Looking at Table 5, it can be noted that the nonmetallized propellant has a much lower flame temperature and much higher mass fractions of the oxidizing species. It is worth remembering that the erosion rate depends primarily on pressure and on chemical attack by H_2O and CO_2, with the flame temperature exerting only a minor influence [1,8]. However, if the flame temperature is low enough, then the recession process may be strongly influenced by chemical kinetics; relatively low flame temperatures, in fact, may result in nozzle surface temperatures of

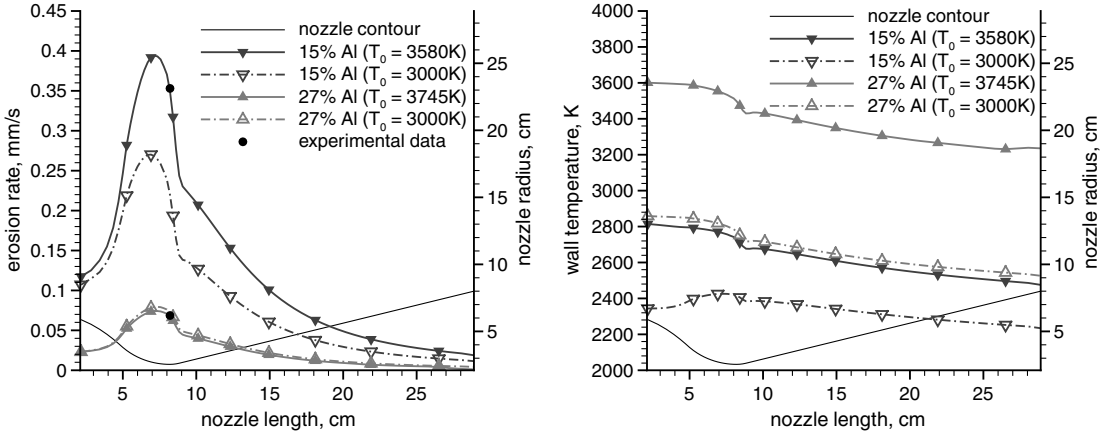

a) Erosion rate distributions **b) Wall temperature distributions**

Fig. 5 Effect of flame temperature variation on a) erosion rate and b) wall temperature (finite-rate model).

about 2000–2500 K, where the influence of chemical kinetics can be very pronounced, hence causing the diffusion-limited model to overestimate recession. Such is the case with the use of non-metallized propellant, as confirmed by Fig. 7a, which shows a pronounced reduction of both the erosion contributions of water vapor and carbon dioxide. The erosion due to OH is instead unaffected by the finite-rate model; nozzle erosion is, hence, diffusion limited with respect to OH, and this can be attributed to the fast reaction of OH with carbon [Eq. (13)]. This is further confirmed by Fig. 7b, which shows that the OH mass fraction reduces to zero at the surface, even with the finite-rate model. The H_2O and CO_2 surface mass fractions are, instead, highly increased in the finite-rate model, denoting a kinetic-limited erosion with respect to these species. Note that their mass fractions are nonzero even in the surface equilibrium approach. This is due to the low surface temperature for which, according to the equilibrium, the oxidizing species are not completely consumed. The surface wall temperature distributions are shown in Fig. 7c, with the surface

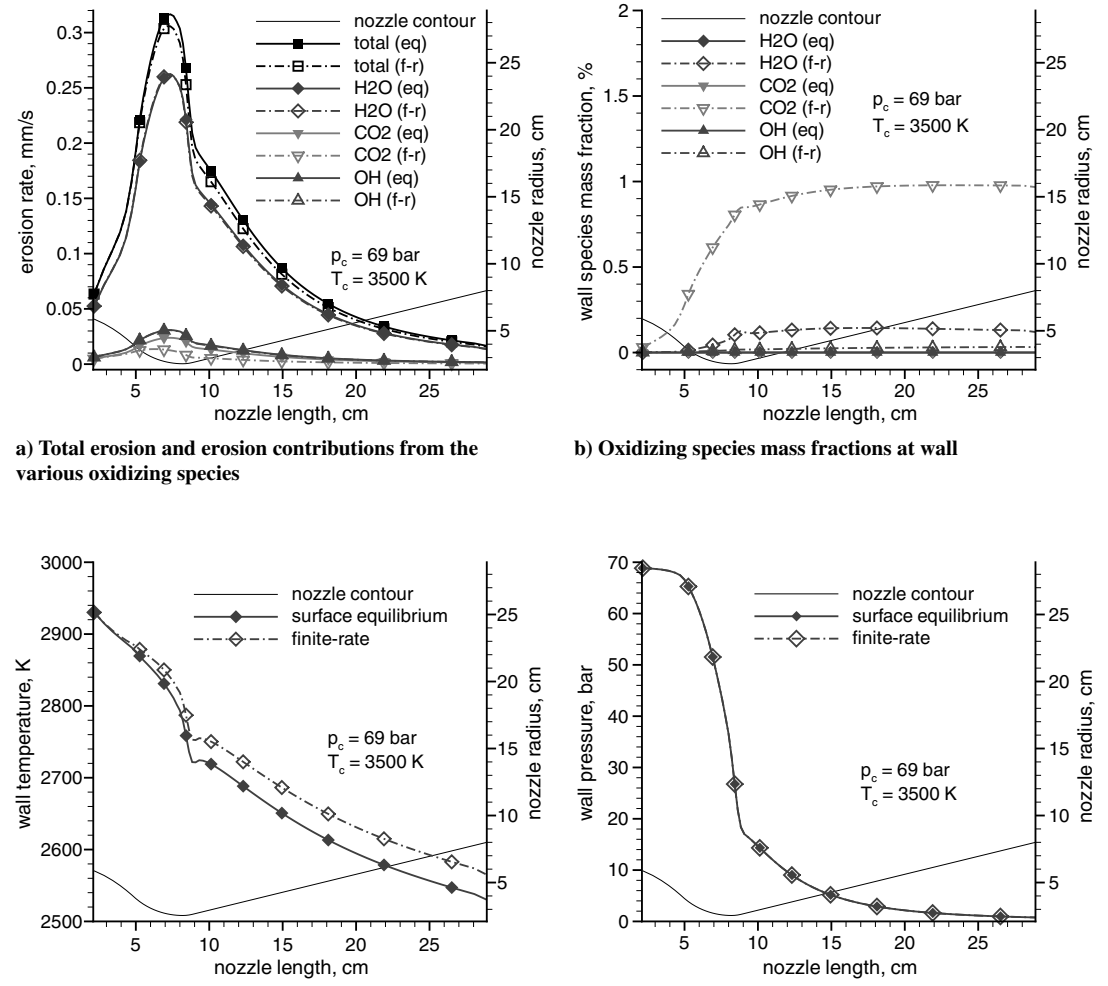

a) Total erosion and erosion contributions from the various oxidizing species **b) Oxidizing species mass fractions at wall**

c) Wall temperature distributions **d) Wall pressure distributions**

Fig. 6 Wall distributions with finite rate and equilibrium model for metallized propellant.

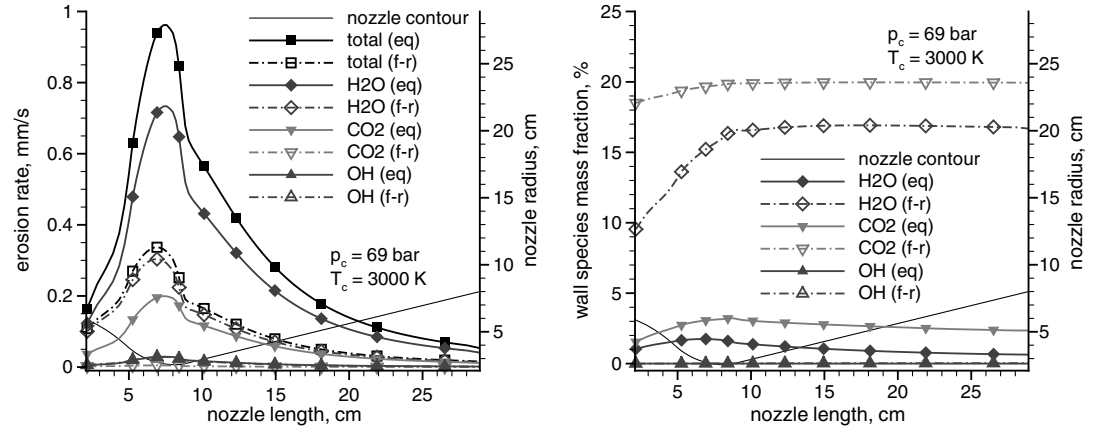

a) Total erosion and erosion contributions from the various oxidizing species

b) Oxidizing species mass fractions at wall

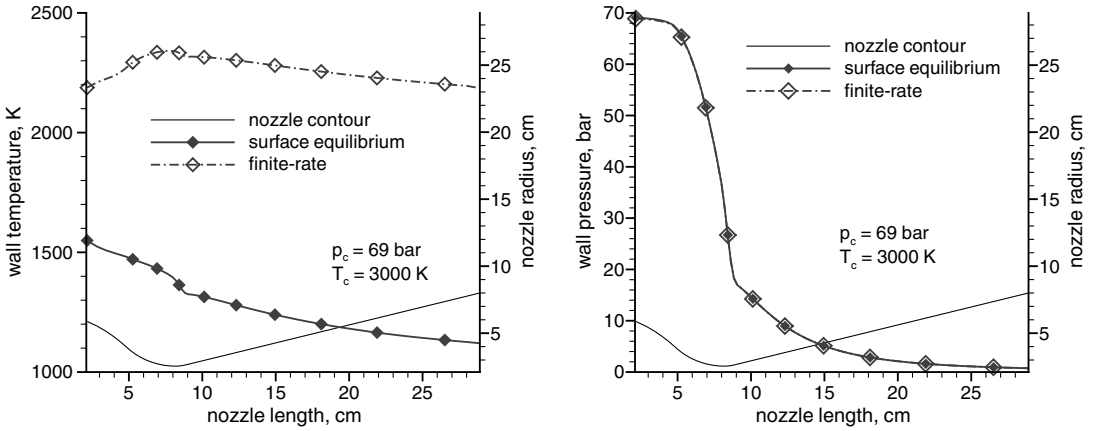

c) Wall temperature distributions

d) Wall pressure distributions

Fig. 7 Wall distributions with finite rate and equilibrium model for nonmetallized propellant.

equilibrium approach producing a very low surface temperature, which is clearly unrealistic. As observed for the metallized propellant case, Fig. 7d confirms that the surface ablation model does not affect the wall pressure distribution.

Figure 8, finally, shows the erosion rate and wall temperature distributions along the nozzle length for the metallized and nonmetallized propellants. The difference between the two cases results from different mechanisms that control the erosion: species diffusion for the metallized propellant and chemical kinetics for the nonmetallized propellant. Even if the flame temperature is much higher for the metallized propellant than for the nonmetallized propellant, the erosion rate is lower for the former than for the latter. This is because aluminum consumes most of the oxygen in the metallized propellant to form Al_2O_3.

V. Conclusions

A general model based on a full Navier–Stokes approach has been developed to examine thermochemical ablation of graphite/carbon–carbon heat protection materials in SRM environments. The model includes the relevant physics of the hot-gas flow, the ablation process, and the internal heat conduction into the material. The two regions,

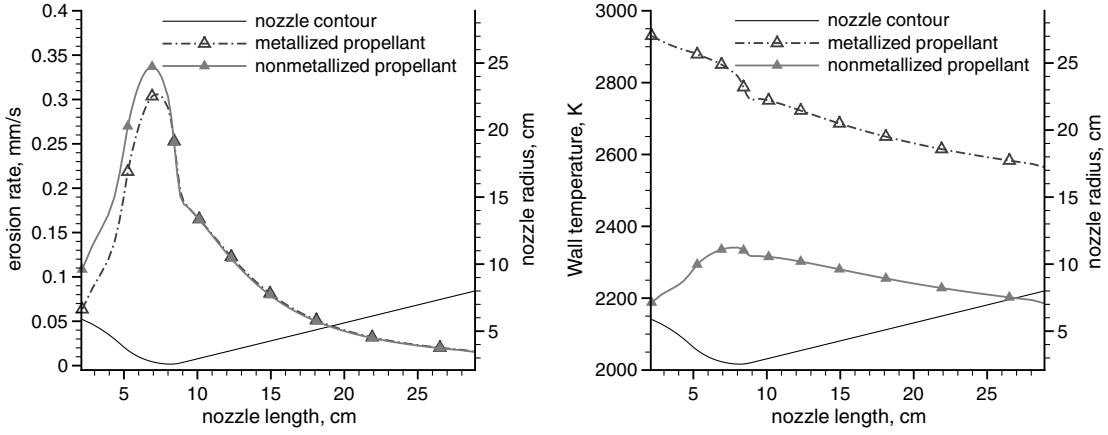

a) Erosion rate distributions

b) Wall temperature distributions

Fig. 8 Erosion rate and wall temperature distributions for metallized and nonmetallized propellants (finite-rate model).

gas and solid, are fully coupled at the surface by appropriate energy and mass balances, allowing the surface conditions to be solved as part of the overall solution. The surface thermochemistry model is based on two different approaches: a surface chemical equilibrium model and a surface nonequilibrium (finite rate) model. The computed results reproduce the expected physical behavior well: for a metallized propellant, the concentrations of the major oxidizing species (H_2O, OH, and CO_2) are substantially reduced in comparison with the nonmetallized propellant due to the formation of aluminum oxides. This effect reduces the thermochemical erosion by these oxidizing species, resulting in a significant reduction of the erosion rates. The analysis of numerical results has also shown that the overall nozzle erosion rate is a function of both the species diffusion rate and the heterogeneous reaction rate at the surface: the erosion rate is found to be dictated by surface chemical kinetics for nonmetallized propellants, for which the wall temperatures are low, and by species diffusion for metallized propellants, for which the surface temperatures are high. Chemical kinetics can have a noticeable effect, even on metallized propellant with low aluminum content, due to their lower surface temperature. The flame temperature is found to be important in determining the nozzle surface temperature that, in turn, can strongly affect the erosion in the kinetic-limited regime, whereas it has almost no effect on the erosion in the diffusion-limited regime. The predicted surface recession rates show an excellent agreement with the available experimental data, with the finite-rate model actually improving the prediction for the low-aluminum-content propellants.

References

[1] Klager, K., "The Interaction of the Efflux of Solid Propellants with Nozzle Materials," *Propellants and explosives*, Vol. 2, No. 3, 1977, pp. 55–63.
doi:10.1002/prep.19770020304

[2] Geisler, R. L., "The Prediction of Graphite Rocket Nozzle Recession Rates," *The 1981 JANNAF Propulsion Meeting*, Chemical Propulsion Information Agency Publ. 342, Vol. 5, Columbia, MD, May 1981, pp. 173–196.

[3] Kuo, K. K., and Keswani, S. T., "A Comprehensive Theoretical Model for Carbon–Carbon Composite Recession," *Combustion Science and Technology*, Vol. 42, Nos. 3–4, 1985, pp. 145–164.
doi:10.1080/00102208508960374

[4] Keswani, S. T., and Kuo, K. K., "Validation of an Aerothermochemical Model for Graphite Nozzle Recession and Heat-Transfer Processes," *Combustion Science and Technology*, Vol. 47, Nos. 3–4, 1986, pp. 177–192.
doi:10.1080/00102208608923872

[5] Borie, V., Brulard, J., and Lengelle, G., "Aerothermochemical Analysis of Carbon-Carbon Nozzle Regression in Solid-Propellant Rocket Motors," *Journal of Propulsion and Power*, Vol. 5, No. 6, 1989, pp. 665–673.
doi:10.2514/3.23204

[6] Acharya, R., and Kuo, K. K., "Effect of Pressure and Propellant Composition on Graphite Rocket Nozzle Erosion Rate," *Journal of Propulsion and Power*, Vol. 23, No. 6, 2007, pp. 1242–1254.
doi:10.2514/1.24011

[7] Thakre, P., and Yang, V., "Chemical Erosion of Carbon–Carbon/Graphite Nozzles in Solid-Propellant Rocket Motors," *Journal of Propulsion and Power*, Vol. 24, No. 4, 2008, pp. 822–833.
doi:10.2514/1.34946

[8] Bianchi, D., Nasuti, F., and Martelli, E., "Coupled Analysis of Flow and Surface Ablation in Carbon–Carbon Rocket Nozzles," *Journal of Spacecraft and Rockets*, Vol. 46, No. 3, 2009, pp. 492–500.
doi:10.2514/1.40197

[9] Geisler, R. L., and Beckman, C. W., "The History of the BATES Motors at the Air Force Rocket Propulsion Laboratories," AIAA Paper 1998-3981, 1998.

[10] Nasuti, F., Martelli, E., Onofri, M., and Pietropaoli, E., "Film Cooling in Dual Bell Nozzle," *Proceedings of the 5th European Symposium on Aerothermodynamics for Space Vehicles, November 2004*, ESTEC, ESA SP-563, Noordwijk, The Netherlands, 2005.

[11] Martelli, E., "Studio Della Fluidodinamica Interna di Ugelli Propulsivi di Tipo Dual Bell," Ph.D. Dissertation, Univ. Degli Studi di Roma "La Sapienza," Rome, Jan. 2006 (in Italian).

[12] Anderson, J. D., *Hypersonic and High Temperature Gas Dynamics*, AIAA, Reston, VA, 2000.

[13] Gordon, S., and McBride, B. J., "Computer Program for Calculation of Complex Chemical Equilibrium Compositions and Applications," NASA RP 1311, 1994.

[14] Moyer, C. B., and Rindal, R. A., "An Analysis of the Chemically Reacting Boundary Layer and Charring Ablator. Part II: Finite Difference Solutions for the In-Depth Response of Charring Materials Considering Surface Chemical and Energy Balances," NASA CR 1061, 1968.

[15] Quan, V., "Quasi-Steady Solution for Ablation-Erosion Heat Transfer," *Journal of Spacecraft and Rockets*, Vol. 7, No. 3, 1970, pp. 355–357.
doi:10.2514/3.29938

[16] Bianchi, D., Nasuti, F., Martelli, E., and Onofri, M., "A Numerical Approach for High-Temperature Flows over Ablating Surfaces," AIAA Paper 2007-4537, 2007.

[17] Bianchi, D., "Modeling of Ablation Phenomena in Space Applications," Ph.D. Dissertation, Univ. Degli Studi di Roma "La Sapienza," Rome, Jan. 2008.

[18] Bianchi, D., Martelli, E., and Nasuti, F., "Coupled Analysis of Flow and Surface Ablation in Carbon–Carbon Rocket Nozzles," AIAA Paper 2008-3912, 2008.

[19] Moretti, G., "A Technique for Integrating Two-Dimensional Euler Equations," *Computers and Fluids*, Vol. 15, No. 1, 1987, pp. 59–75.
doi:10.1016/0045-7930(87)90005-3

[20] Nasuti, F., and Onofri, M., "Analysis of Unsteady Supersonic Viscous Flows by a Shock Fitting Technique," *AIAA Journal*, Vol. 34, No. 7, 1996, pp. 1428–1434.
doi:10.2514/3.13249

[21] Nasuti, F., and Onofri, M., "Analysis of In-Flight Behavior of Truncated Plug Nozzles," *Journal of Propulsion and Power*, Vol. 17, No. 4, July–Aug. 2001, pp. 809–817.
doi:10.2514/2.5837; alsoAIAA Paper 2000–3289, 2000.

[22] Spalart, P. R., and Allmaras, S. R., "A One-Equation Turbulence Model for Aerodynamic Flow," *La Recherche Aerospatiale: Bulletin Bimestriel de l'Office National D'etudes et de Recherches Aerospatiales*, Vol. 1, 1994, pp. 5–21.

[23] Geisler, R. L., "The Relationship Between Solid Propellant Formulation Variables and Nozzle Recession Rates," *JANNAF Rocket Nozzle Technology Subcommittee Meeting*, Joint Army Navy NASA Air Force, July 1978.

[24] Evans, B., Kuo, K. K., Ferrara, P. J., Moore, J. D., Kutzler, P., and Boyd, E., "Nozzle Throat Erosion Characterization Study Using a Solid-Propellant Rocket Motor Simulator," 43rd AIAA/ASME/SAE/ASEE Joint Propulsion Conference and Exhibit, AIAA Paper 2007-5776, July 2007.

S. Son
Associate Editor